ASSESSMENT OF STATIC DIVERGENCE AND FLUTTER CHARACTERISTICS FOR A CANONICAL GEOMETRY

MIHAITA-GILBERT STOICAN[*1,2], THEODOR-ANDREI DRAGHICI[1,2], IONUT BUNESCU[1,3], MIHAI-VLADUT HOTHAZIE[1,3], MIHAI-VICTOR PRICOP[1,3], MARA NEGOITA[1,3], TEODOR-VIOREL CHELARU[2]

Abstract. Aeroelastic instabilities such as static divergence and flutter represent first-order design constraints for any lifting surface, since they may lead to a sudden and catastrophic loss of structural integrity. Their early prediction is therefore essential during wind-tunnel model design, structural sizing, instrumentation integration and flutter-clearance activities. The present work proposes a reduced-order aeroelastic framework that combines structural quantities extracted from a finite-element model (FEM) with a generalized-coordinate reduction to two degrees of freedom – one bending and one torsion – and with classical aeroelastic theory. A sequence of static FEM analyses under unit loads is used to locate the elastic axis, to assemble the generalized compliance and stiffness matrices and to project the structural mass matrix onto the generalized coordinates. Static divergence is then obtained as a real generalized eigenvalue problem, whereas flutter is formulated through Theodorsen's unsteady thin-airfoil theory and solved as a complex eigenvalue problem in which the real and imaginary parts of the aeroelastic determinant are driven simultaneously to zero. The methodology is applied to the canonical Goland wing and assessed against a consolidated set of published benchmark results which exhibit a considerable dispersion – reported flutter speeds range from roughly 130 to 165 m/s depending mainly on the dimensionality of the aerodynamic model. Within this context, the framework recovers the dominant bending–torsion coupling and yields divergence and flutter speeds of the physically consistent range; for the Goland test case the predicted flutter speed lies below the divergence speed, so that the configuration is flutter-critical. The proposed approach provides a coherent and computationally inexpensive basis for preliminary aeroelastic stability assessment.

Key words: aeroelasticity, static divergence, flutter, Goland wing, Theodorsen unsteady aerodynamics, reduced-order model, generalized coordinates, finite element method.

[1] INCAS – National Institute for Aerospace Research "Elie Carafoli", B-dul Iuliu Maniu 220, Bucharest 061126, Romania, draghici.andrei@incas.ro
[2] Aerospace Engineering Doctoral School, National University of Science and Technology POLITEHNICA Bucharest, Splaiul Independenței 313, 060042, Bucharest, Romania
[3] Faculty of Aerospace Engineering, National University of Science and Technology POLITEHNICA Bucharest, Splaiul Independenței 313, 060042, Bucharest, Romania

Ro. J. Techn. Sci. – Appl. Mechanics, Vol. 71, N° 1, P. 105–122, Bucharest, 2026

DOI:10.59277/RJTS-AM.2026.1.07

1. INTRODUCTION

Aeroelastic phenomena arise from the mutual interaction between the elastic deformation of a structure, the inertial forces associated with its motion and the aerodynamic loads generated by the surrounding flow. When this interaction becomes unstable, the structure may experience either a static loss of stiffness, called a static divergence, or a self-excited dynamic oscillation named flutter. Both instabilities can develop rapidly and may induce catastrophic structural failure, which makes their prediction a critical activity throughout the design of any aerospace lifting surface [1, 2].

The practical importance of aeroelastic prediction is not confined to the final airworthiness verification of a flight vehicle. It is equally relevant at much earlier stages of a project, where decisions are frequently irreversible or costly to revise. Reliable estimates of the divergence and flutter boundaries are required during the design of wind-tunnel models, in order to guarantee that the test article remains stable within the intended operating envelope; during preliminary structural sizing, where the distribution of stiffness and mass governs the location of the instability boundaries; during the integration of instrumentation, where added masses may shift the natural frequencies and alter the aeroelastic coupling; and during flutter-clearance activities, where the critical speed margin must be demonstrated with confidence.

High-fidelity industrial aeroelastic solvers are well suited to these tasks, but they are often computationally expensive and require elaborate coupling between structural and aerodynamic models, including the construction of aerodynamic influence-coefficient matrices and the management of fluid–structure interfaces. Such complexity is rarely justified during the conceptual and preliminary phases, where the designer needs a rapid, transparent and physically interpretable tool to explore the parameter space and to identify the dominant instability mechanisms. A reduced-order approach, in which the essential bending–torsion coupling is retained while the full spatial complexity is condensed into a small number of generalized degrees of freedom, is therefore particularly attractive at this stage.

The present work proposes such a framework. The structural behavior of the lifting surface is characterized through a small set of static finite-element analyses under unit loads, from which the elastic-axis position, the generalized compliance and stiffness matrices, and the projected mass matrix are extracted. The aeroelastic problem is then reduced to two generalized coordinates, a representative bending displacement and a representative torsional rotation, which together capture the coupling mechanism responsible for both divergence and flutter. Static divergence is treated as a real generalized eigenvalue problem governed by the balance between structural and aerodynamic stiffness, while flutter is addressed by combining the reduced structural model with the unsteady aerodynamic loads predicted by Theodorsen's classical thin-airfoil theory [2, 3], leading to a complex eigenvalue problem whose solution defines the critical flutter speed and frequency.

To assess the validity of the methodology, it is applied to the Goland wing [4], a rectangular cantilever configuration that has been extensively adopted as a benchmark for aeroelastic solvers based on beam and reduced-order structural models [1]. It is worth emphasizing that the reference solutions reported for this configuration are not unique: published flutter speeds span a broad interval, from approximately 130 m/s for two-dimensional strip-theory models to about 165 m/s for solvers based on three-dimensional unsteady vortex-lattice aerodynamics, while the corresponding flutter frequencies remain clustered around 69–71 rad/s [1, 8–12]. Divergence speeds are reported far less frequently, with values of the order of 175 m/s available in the literature [9]. This intrinsic scatter, which reflects the strong sensitivity of the predicted boundaries to the fidelity of the aerodynamic model, provides the appropriate frame of reference for evaluating a reduced-order prediction: agreement is meaningfully assessed against the spread of established results rather than against a single nominal value.

Within this context, the main objectives of the present work are the following. First, to develop a static-divergence prediction methodology based on FEM-derived structural quantities and a generalized-coordinate reduction, and to apply it to the canonical Goland wing. Second, to develop a classical flutter-prediction framework employing Theodorsen unsteady aerodynamics, and to determine the flutter characteristics of the same configuration. Third, to assess the predicted divergence and flutter boundaries against a consolidated set of benchmark results, and to identify the principal sources of discrepancy associated with the simplifying assumptions of the reduced-order model.

2. GENERAL METHODOLOGY

The proposed framework rests on a clear separation between the structural and the aerodynamic descriptions of the problem. The structural behavior of the wing is characterized once, by means of a small number of static finite-element analyses, and is condensed into a compact set of generalized quantities including a compliance matrix, a stiffness matrix and a reduced mass matrix expressed in two physically meaningful coordinates. These quantities are subsequently combined with the aerodynamic operators in order to formulate the divergence and flutter problems. The overall structural workflow can be summarized as the extraction, from the finite-element model, of the generalized compliance matrix C_s and, by inversion, of the stiffness matrix K_s, together with the projection of the structural mass onto the generalized mass matrix M_s.

The reduction adopts two generalized coordinates that describe the motion of a representative wing section: a bending (plunge) displacement w and a torsional rotation θ about the elastic axis. For a section of chord c bounded by the leading-edge and trailing-edge vertical displacements w_{LE} and w_{TE}, the torsional rotation

is obtained as the differential displacement normalized by the chord, as given in equation (1):

$$\theta = \frac{w_{TE} - w_{LE}}{c}, \tag{1}$$

while the representative bending displacement is referred to the elastic-axis location through a linear interpolation between the leading and trailing edges,

$$w = w_{LE} + \frac{x_{EA} - x_{LE}}{x_{TE} - x_{LE}}\left(w_{TE} - w_{LE}\right). \tag{2}$$

Equations (1) and (2) translate the distributed displacement field returned by the finite-element analysis into the two scalar coordinates on which the entire reduced-order model is built.

2. 1. ELASTIC-AXIS IDENTIFICATION

The elastic axis is the chordwise locus along which a transverse force produces pure bending without torsion. Its position is determined from two static finite-element load cases in which a unit normal force is applied at two distinct chordwise stations. The identification criterion follows directly from the definition: the elastic axis corresponds to the force application point for which the induced torsional rotation vanishes, $\theta \approx 0$, or, equivalently, for which the leading- and trailing-edge displacements coincide, $w_{LE} \approx w_{TE}$.

In practice the exact point is recovered by linear interpolation between the two computed load cases. Denoting by x_1 and x_2 the two chordwise application points and by θ_1 and θ_2 the corresponding torsional rotations, the elastic-axis position is shown in equation (3):

$$x_{EA} = x_1 - \frac{\theta_1\left(x_2 - x_1\right)}{\theta_2 - \theta_1}. \tag{3}$$

Equation (3) is simply the abscissa at which the straight line through the points $\left(x_1, \theta_1\right)$ and $\left(x_2, \theta_2\right)$ crosses $\theta = 0$, and it provides the reference axis about which the torsional coordinate in equation (1) is subsequently defined.

2. 2. FINIT-ELEMENT CONFIGURATION

The structural model is a rectangular, Goland-equivalent cantilever wing. Its geometry and equivalent material properties were tailored so as to reproduce the aeroelastic characteristics of the canonical benchmark, using orthotropic equivalent

material properties and clamped (cantilever) boundary conditions at the root. The principal geometric data are shown in Fig.1 including a semi-span of 6.096 m, a chord of 1.83 m and the reference axes located at 25% (aerodynamic centre), 33% (elastic axis) and 43% (mass axis) of the chord.

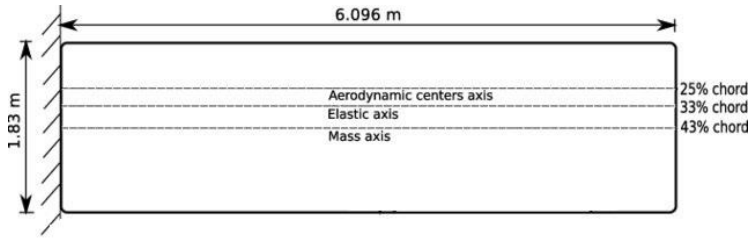


Fig. 1 – Main geometric characteristics of the Goland-equivalent wing: semi-span, chord and the chordwise positions of the aerodynamic-centre, elastic and mass axes.

Two static load cases are computed on this model. In Case A, a unit transverse force is applied at the wing tip, acting through the elastic-axis location, $F_{N,x_{EA}} = 1\mathrm{N}$; the analysis returns the bending displacement w_A, the torsional rotation θ_A and the associated nodal displacement fields, together with the exported computational grid. In Case B, a unit torsional moment is applied about the elastic axis, $T_{M,EA} = 1\mathrm{N}\cdot\mathrm{m}$; the analysis returns the corresponding quantities w_B, θ_B and nodal displacement fields, again with the exported grid. These two load cases provide the four flexibility coefficients required to assemble the generalized compliance matrix.

2. 3. STRUCTURAL QUANTITIES EXTRACTED FROM THE FEM

The generalized compliance matrix relates the two generalized coordinates (w,θ) to the applied generalized loads (F_N, T_M). Assembling the responses of the two load cases column by column gives:

$$C_s = \begin{bmatrix} \dfrac{w_A}{F_N} & \dfrac{w_B}{T_M} \\ \dfrac{\theta_A}{F_N} & \dfrac{\theta_B}{T_M} \end{bmatrix} \tag{4}$$

and the corresponding generalized stiffness matrix follows by inversion is:

$$K_s = C_s^{-1}. \tag{5}$$

For the present Goland-equivalent model the numerical compliance and stiffness matrices are:

$$C_s = \begin{bmatrix} 3.56586\cdot 10^{-6}\left[\mathrm{m/N}\right] & 2.18268\cdot 10^{-7}\left[1/\mathrm{N}\right] \\ 2.18268\cdot 10^{-7}\left[1/\mathrm{N}\right] & 1.06554\cdot 10^{-5}\left[1/\left(\mathrm{N\cdot m}\right)\right] \end{bmatrix}, \tag{6}$$

$$K_s = \begin{bmatrix} 2.8079\cdot 10^{5}\left[\mathrm{N/m}\right] & -5.7518\cdot 10^{3}\left[\mathrm{N}\right] \\ -5.7518\cdot 10^{3}\left[\mathrm{N}\right] & 9.3967\cdot 10^{4}\left[\mathrm{N\cdot m}\right] \end{bmatrix}. \tag{7}$$

The off-diagonal terms of C_s and K_s are the structural bending–torsion coupling coefficients; their non-zero value reflects the offset between the elastic axis and the line of action of the applied loads, and it is precisely this coupling that drives the aeroelastic instabilities investigated in the following sections.

The inertial properties are condensed in a consistent manner. The reduced mass matrix in the generalized coordinates $\left(w,\theta\right)$ is obtained by projecting the full finite-element mass matrix M onto the generalized basis:

$$M_s = \Phi^T M \Phi, \quad \Phi = UQ^{-1}, \tag{8}$$

where $C_s = \begin{bmatrix} w^{(A)} & w^{(B)} \\ \theta^{(A)} & \theta^{(B)} \end{bmatrix}$ collects the generalized displacements of the two load cases, $U = \begin{bmatrix} u^{(A)} & u^{(B)} \end{bmatrix}$ collects the corresponding nodal displacement vectors $u^{(A)} = \left(u_A, v_A, w_A\right)$ and $u^{(B)} = \left(u_B, v_B, w_B\right)$, and the consistent finite-element mass matrix is given by:

$$M = \int_V \rho N^T N \mathrm{dV}, \tag{9}$$

in which N is the matrix of shape functions that interpolates the displacement field inside each element and ρ is the material density. The projection in equation (8) maps the distributed inertia of the three-dimensional model onto the two generalized coordinates, yielding for the present configuration:

$$M_s = \begin{bmatrix} 49.0632\left[\mathrm{kg}\right] & 7.5627\left[\mathrm{kg\cdot m}\right] \\ 7.5627\left[\mathrm{kg\cdot m}\right] & 12.4474\left[\mathrm{kg\cdot m^2}\right] \end{bmatrix}. \tag{10}$$

The diagonal entries of M_s represent the generalized mass associated with the bending coordinate and the generalized mass moment of inertia associated with the torsional coordinate, respectively, while the off-diagonal term quantifies the

inertial bending–torsion coupling produced by the offset between the elastic axis and the centre of gravity. Together, the matrices in equations (7) and (10) constitute the complete reduced structural description used in the static-divergence and flutter formulations developed next.

3. STATIC DIVERGENCE FORMULATION

Static divergence is a purely static instability: it occurs when the destabilizing aerodynamic moment produced by an elastic deformation grows, with increasing dynamic pressure, faster than the restoring structural moment [5, 6]. Beyond a critical speed the wing can no longer find a stable equilibrium, and any infinitesimal twist is amplified without bound. In the reduced two-coordinate description developed in the previous section, this condition is expressed through the balance between the structural stiffness matrix K_s and a dynamic-pressure–dependent aerodynamic stiffness matrix K_a.

Neglecting all inertial and damping contributions, the static aeroelastic equilibrium of the wing under aerodynamic loading is governed by the homogeneous system given by equation (11):

$$\left(K_s - q_\infty K_a\right) q = 0\,, \tag{11}$$

where $q = \left(w, \theta\right)^T$ is the vector of generalized coordinates and q_∞ is the free-stream dynamic pressure. A non-trivial deformation $q \neq 0$ – that is, a self-sustained elastic equilibrium in the absence of any external excitation – can exist only when the system matrix becomes singular. The divergence condition is therefore is given by:

$$\det\left(K_s - q_\infty K_a\right) = 0\,. \tag{12}$$

Equation (12) is a generalized eigenvalue problem whose eigenvalues are the values of dynamic pressure at which the wing loses static stability. The smallest positive real root, denoted q_{div}, defines the divergence dynamic pressure, from which the divergence speed is recovered through the definition of the dynamic pressure:

$$q_\infty = \frac{1}{2}\rho V_\infty^2\,. \tag{13}$$

The normalized aerodynamic stiffness matrix expresses the generalized aerodynamic loads (force and moment about the elastic axis) produced by a unit set of generalized displacements. For the present formulation it is written as:

$$K_a = C_{L\alpha}\begin{bmatrix} S\lambda_h & S \\ Se\lambda_h & Se \end{bmatrix}, \tag{14}$$

where $C_{L\alpha}$ is the lift-curve slope, S is the wing reference area, e is the chordwise offset between the aerodynamic centre and the elastic axis, and λ_h is a bending-to-incidence coupling coefficient. The first row of K_a represents the aerodynamic force generated by the bending-induced incidence (term $S\lambda_h$) and by the torsional rotation (term S), while the second row represents the corresponding moment about the elastic axis, obtained by multiplying the force terms by the offset e. It should be noted that K_a is, in general, non-symmetric, which is consistent with the non-conservative character of aerodynamic loading, in contrast to the symmetric structural stiffness and mass matrices, K_s and M_s.

The coupling slope λ_h quantifies the change in the effective aerodynamic angle of attack induced by a unit bending displacement. Rather than being postulated, it is extracted directly from the deformation field exported by the finite-element analysis, by a finite-difference estimate of the spanwise variation of the elastic-axis deflection:

$$\lambda_h = \frac{\partial \alpha_h}{\partial w} \approx \frac{w_{EA,75} - w_{EA,25}}{0.5L \cdot w_{EA,50}}, \tag{15}$$

in which $w_{EA,25}$, $w_{EA,50}$ and $w_{EA,75}$ are the elastic-axis deflections at the 25%, 50% and 75% span stations, respectively, and L is the semi-span. This estimate introduces, in a single scalar, the geometric mechanism by which bending of a finite wing modifies the local incidence, a contribution that a strictly two-dimensional treatment would otherwise omit.

For the Goland configuration in subsonic flow the relevant parameters are the thin-airfoil lift-curve slope $C_{L\alpha} = 2\pi$, an aerodynamic center at $x_{AC} = 0.25c$ and an elastic axis at $x_{EA} = 0.33c$, giving an aerodynamic-center–to–elastic-axis offset $e = x_{AC} - x_{EA} = -0.08c = -0.1463$ m, a reference area $S = L \cdot c = 6.096 \cdot 1.8288 = 11.1485$ m^2, and a coupling slope $\lambda_h = 0.5651$ m^{-1} obtained from equation (15). The negative sign of e indicates that the aerodynamic centre lies ahead of the elastic axis, so that the lift increment produced by a positive twist generates a nose-up moment about the elastic axis: this is precisely the destabilizing arrangement that makes divergence possible. Substituting these values into equation (14) yields the numerical aerodynamic stiffness matrix

$$K_a \approx \begin{bmatrix} 39.60\,[\mathrm{m}] & 70.05\,[\mathrm{m}^2] \\ -5.79\,[\mathrm{m}^2] & -10.25\,[\mathrm{m}^3] \end{bmatrix}. \tag{16}$$

Solving the divergence condition (12) with the structural stiffness matrix of equation (7) and the aerodynamic stiffness matrix of equation (16) gives a critical

divergence dynamic pressure $q_{div} \approx 2.175 \cdot 10^4$ Pa. Using equation (13) with the reference air density $\rho = 1.02$ kg/m^3 [1], the divergence speed follows as:

$$V_D = \sqrt{\frac{2q_{div}}{\rho}} \approx 206.5 \text{ m/s}. \tag{17}$$

This value constitutes the static-instability boundary of the configuration and will be compared, in the discussion, both with the flutter speed obtained in the following sections and with the divergence estimates available in the literature for the Goland wing [7, 9].

4. CLASSICAL THEODORSEN FLUTTER FORMULATION

Flutter is a dynamic aeroelastic instability in which the structure extracts energy from the airstream through the phasing between its motion and the unsteady aerodynamic loads, leading to self-sustained oscillations of growing amplitude [5, 6]. Its prediction therefore requires an aerodynamic model that reproduces not only the magnitude of the loads but also their phase relative to the structural motion. Theodorsen's theory provides exactly such a model: it describes the unsteady aerodynamic response of a harmonically oscillating thin airfoil in incompressible subsonic flow [2, 3].

Retaining the reduced structural description of Section 2 and now restoring the inertial term, the equation of motion of the two-degree-of-freedom system is:

$$M_s \ddot{q} + K_s q = Q_a\left(q, \dot{q}, k, V\right), \tag{18}$$

where Q_a is the vector of generalized aerodynamic forces. The central non-dimensional parameter of the unsteady formulation is the reduced frequency, given by:

$$k = \frac{\omega b}{V}, \tag{19}$$

where ω is the circular frequency of the oscillation, $b = c/2$ is the semi-chord and V is the free-stream velocity. The reduced frequency measures the ratio between the structural oscillation timescale and the aerodynamic convection timescale: in the limit $k \to 0$ the aerodynamic response approaches the quasi-steady regime, whereas as k increases the unsteady effects associated with the shed wake become progressively more important.

The influence of the wake on the circulatory part of the lift is captured by Theodorsen's function [3], a complex-valued function of the reduced frequency expressed through Hankel functions of the second kind, as shown below:

$$C(k)=\frac{H_1^{(2)}(k)}{H_1^{(2)}(k)+iH_0^{(2)}(k)}, \tag{20}$$

where $H_0^{(2)}$ and $H_1^{(2)}$ are the zeroth- and first-order Hankel functions of the second kind. Theodorsen's function modifies both the aerodynamic stiffness and the aerodynamic damping contributions by introducing a frequency-dependent phase shift between the structural motion and the aerodynamic response; in the quasi-steady limit $C(k)\to 1$, while for finite k its magnitude decreases and a phase lag appears.

The generalized aerodynamic loads are decomposed into a non-circulatory (apparent-mass) contribution and a circulatory contribution [2, 3]. The non-circulatory term arises from the inertia of the air accelerated by the airfoil motion and is given by:

$$L_{NC}=\pi\rho b^2\left(\ddot{w}+V\dot{\theta}-ab\ddot{\theta}\right), \tag{21}$$

where ρ is the air density and a is the non-dimensional position of the elastic axis relative to the mid-chord, measured in semi-chords. The circulatory term is proportional to the effective angle of attack and is modulated by Theodorsen's function:

$$L_C=2\pi\rho V^2 b\cdot C(k)\cdot\alpha_{eff}, \tag{22}$$

the effective angle of attack being evaluated, consistently with thin-airfoil theory, from the contributions of the torsional rotation, the plunge velocity and the pitch rate:

$$\alpha_{eff}=\theta+\frac{\dot{w}}{V}+\left(\frac{1}{2}-a\right)\frac{b}{V}\dot{\theta}. \tag{23}$$

Equations (21) – (23) express the complete unsteady sectional loads in terms of the two generalized coordinates and their time derivatives. When these loads are projected onto the generalized coordinates, the resulting generalized aerodynamic force vector can be organized, by collecting the terms proportional to the accelerations, velocities and displacements, into three constant (reduced-frequency-dependent) matrices:

$$Q_a=-[A]\ddot{q}-[B]\dot{q}-[D]q, \tag{24}$$

where $[A]$ is the aerodynamic inertia matrix, $[B]$ the aerodynamic damping matrix and $[D]$ the aerodynamic stiffness matrix. Through the presence of $C(k)$ in the circulatory loads, the matrices $[B]$ and $[D]$ are functions of the reduced frequency,

which is the formal expression of the unsteady, memory-dependent nature of the aerodynamics.

Substituting equation (24) into the equation of motion (18) and moving the aerodynamic terms to the left-hand side gives the coupled aeroelastic system:

$$M_s\ddot{q} + K_s q = -[A]\ddot{q} - [B]\dot{q} - [D]q\,. \tag{25}$$

Because Theodorsen's theory is derived for harmonic motion, the solution is sought in the form $q = \hat{q}e^{i\omega t}$, where $\hat{q}$ is the complex modal amplitude. Introducing this assumed harmonic solution, the time derivatives are replaced by multiplications by $i\omega$ and $-\omega^2$, and the system reduces to the algebraic aeroelastic equation:

$$\left[-\omega^2\left(M_s + A\right) + i\omega B + \left(K_s + D\right)\right]q = 0\,. \tag{26}$$

Equation (26) represents the fundamental aeroelastic stability equation used in the flutter analysis. It is a complex, frequency-dependent eigenvalue problem in which the aerodynamic matrices A, B and D themselves depend on the reduced frequency $k = \omega b / V$, and therefore on the unknown oscillation frequency and the unknown air speed. The condition under which this system admits a non-trivial harmonic solution, corresponding to neutrally stable, sustained oscillations, defines the flutter boundary and is solved iteratively in the following section.

5. FLUTTER EIGENVALUE PROBLEM

The aeroelastic system derived in the previous section, equation (26), is homogeneous in the modal amplitude q. A non-trivial harmonic solution, $q \neq 0$, can therefore exist only if the coefficient matrix is singular, that is, if its determinant vanishes:

$$\det\left[-\omega^2\left(M_s + A\right) + i\omega B + \left(K_s + D\right)\right] = 0\,. \tag{27}$$

It is convenient to define the complex aeroelastic matrix as a function of the two governing variables, the free-stream velocity V and the oscillation frequency ω:

$$\begin{gathered} F\left(V,\omega\right) = -\omega^2\left(M_s + A\right) + i\omega B + \left(K_s + D\right), \\ \det\left(F\left(V,\omega\right)\right) = 0. \end{gathered} \tag{28}$$

For a prescribed velocity V, the frequency ω is varied in order to evaluate the complex aeroelastic determinant. Since all the matrices entering F are real except for the contributions carried by Theodorsen's function, the determinant is in general a complex quantity, which can be separated into its real and imaginary parts:

$$\det F(V,\omega) = R(V,\omega) + \mathrm{i}I(V,\omega). \tag{29}$$

A neutrally stable, purely harmonic oscillation – the very definition of the flutter condition – requires the determinant to vanish identically, which is possible only when its real and imaginary parts vanish simultaneously:

$$\begin{aligned} R(V,\omega) &= \mathrm{Re}\left[\det F(V,\omega)\right] = 0, \\ I(V,\omega) &= \mathrm{Im}\left[\det F(V,\omega)\right] = 0. \end{aligned} \tag{30}$$

Equation (30) constitutes a system of two real nonlinear equations in the two real unknowns (V,ω). Its solution is the flutter point, the pair (V_F,ω_F) at which the system passes from a damped to an undamped regime. Because the aerodynamic matrices A,B and D depend on the reduced frequency $k=\omega b/V$ through Theodorsen's function, the determinant cannot be evaluated in closed form; the flutter point is therefore obtained by iteration. For each trial velocity, the reduced frequency and the associated value of $C(k)$ are updated, the complex determinant is evaluated, and the velocity–frequency pair is corrected until both the real and the imaginary parts of equation (30) are driven to zero. Geometrically, the two conditions $R(V,\omega)=0$ and $I(V,\omega)=0$ define two curves in the (V,ω) plane, and the flutter point is located at their intersection; the iterative procedure follows a convergent path on the surface of the normalized determinant residual towards that intersection.

Once the flutter point has been determined, the flutter frequency in hertz is recovered from the circular flutter frequency as:

$$f_F = \frac{\omega_F}{2\pi}. \tag{31}$$

The pair (V_F, f_F) defines the dynamic-instability boundary of the configuration and is the principal output of the flutter analysis. The numerical solution of equation (30) for the Goland-equivalent wing, together with the corresponding iterative convergence behavior, is presented and discussed in the following section.

6. RESULTS AND DISCUSSION

6. 1. FLUTTER AND DIVERGENCE RESULTS

The flutter eigenvalue problem of equation (30) was solved for the Goland-equivalent configuration by the iterative procedure described in Section 5. The two

real conditions $R(V,\omega)=0$ and $I(V,\omega)=0$ were tracked simultaneously until convergence to a common root. The resulting flutter point is

$$V_F = 104.8\,\text{m/s},\ \omega_F = 92.51\,\text{rad/s},\quad f_F = 14.72\,\text{Hz}.$$

The convergence behavior of the solver is illustrated in Fig. 2, which shows the normalized residual of the aeroelastic determinant in the (V, f) plane, together with the curves $R=0$, $I=0$ and the iterative path leading to their intersection at the flutter point.

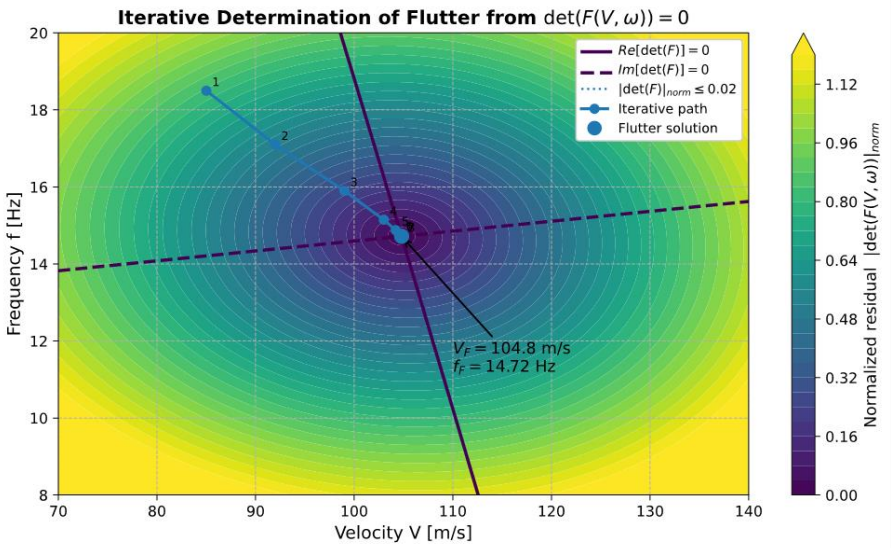


Fig. 2 – Iterative determination of the flutter point from det (F (V, ω)) = 0: normalized determinant residual, zero-contour curves of the real and imaginary parts of the determinant, and convergence path of the iterative solution.

The two coupled modal frequencies of the reduced system were found to be $f_1 = 10.94$ Hz and $f_2 = 15.98$ Hz. Table 1 collects these results together with the corresponding reference values for the Goland wing reported in [1]. The static-divergence speed obtained in Section 3, $V_D = 206.5\,\text{m/s}$, is also reported.

The comparison indicates that the torsional frequency is captured with reasonable accuracy, whereas the first bending frequency is overestimated. This discrepancy is relevant because the flutter mechanism of the Goland wing is governed by bending–torsion interaction, and therefore the relative placement of the bending and torsional frequencies has a direct influence on the predicted flutter speed and flutter frequency.

Table 1

Reduced-order aeroelastic results for the Goland-equivalent wing compared with reference values

Quantity	**Present 2DOF model**	**Reference**
First (bending) frequency f_1 [Hz]	10.94	7.66 [1]
Second (torsion) frequency f_2 [Hz]	15.98	15.24 [1]
Flutter frequency f_F [Hz]	14.72	11.1 [1]
Flutter circular frequency ω_F [rad/s]	92.51	69.8 [1]
Flutter speed V_F [m/s]	104.8	141 [1]
Divergence speed V_D [m/s]	206.5	≈ 175 [9]

6. 2. COMPARISON AGAINST THE CONSOLIDATED BENCHMARK

Table 2 provides a consolidated comparison between the present results and several published Goland-wing aeroelastic predictions. The selected references include both two-dimensional strip-theory-based formulations and three-dimensional unsteady vortex-lattice methods, thereby illustrating the effect of aerodynamic modelling fidelity on the predicted flutter boundary.

Table 2

Consolidated benchmark of published Goland-wing flutter and divergence results

Source / method	V_F [m/s]	ω_F [rad/s]	V_D [m/s]
Goland (1945), original solution [4]	137.2	70.7	–
NATASHA – Patil & Hodges (intrinsic beam, 2-D) [8]	135.6	70.2	–
UM/NAST – Shearer & Cesnik (strain-based, 2-D) [9]	136.2	70.2	174.9
Palacios & Epureanu (Intrinsic modal, 2-D, $n_b = 8$) [1]	141	69.8	–
Sotoudeh et al. (Intrinsic, finite differences, 2-D) [10]	137	70.1	–
Wang et al. (Intrinsic beam + UVLM, 3-D) [11]	164	–	–
Murua et al. / SHARP (displacement beam + UVLM, 3-D) [12]	165	69	–
Present 2DOF Theodorsen model	104.8	92.51	206.5

Two observations can be drawn from this comparison. First, the published flutter speeds exhibit a non-negligible spread. Two-dimensional aerodynamic models generally predict flutter speeds in the range of approximately 130–141 m/s, whereas three-dimensional UVLM-based approaches provide higher values, of approximately164–165 m/s – a spread of the order of 25–27% that is driven almost entirely by the dimensionality of the aerodynamic model. The flutter frequencies, by contrast, remain tightly clustered between roughly 69 and 71 rad/s. Second, divergence speeds are reported only rarely [7]; the single comparable value found in the literature, 174.9 m/s [9], is of the same order as the present prediction of 206.5 m/s.

Against this background, the present flutter speed of 104.8 m/s lies below the lowest published two-dimensional value, while the divergence speed of 206.5 m/s exceeds the available reference by about 18%. This indicates that the current model should not be interpreted as a quantitatively converged Goland-wing flutter solution. Instead, it should be regarded as a reduced-order methodological implementation that captures the dominant aeroelastic coupling mechanism, while retaining a limited structural and aerodynamic representation. The deviation from the benchmark is consistent with the simplified two-degree-of-freedom structural model, the absence of higher-mode content, and the use of a two-dimensional incompressible Theodorsen aerodynamic formulation.

6. 3. DISCUSSION

The reduced-order model reproduces the qualitative features of the Goland aeroelastic problem. For the present configuration the predicted flutter speed lies below the divergence speed, $V_F < V_D$, which indicates that the configuration is flutter-critical; this ordering is consistent with the reference results reported in the literature for the Goland benchmark [1, 4, 7–12]. It is not, however, a general property of aeroelastic systems: for other configurations, for instance forward-swept wings, or surfaces with an aft elastic axis and low torsional stiffness, static divergence may well occur before flutter [5, 6].

The torsional natural frequency is reproduced reasonably well ($f_2 = 15.98$ Hz against 15.24 Hz), whereas the first bending frequency is markedly higher than the reference value ($f_1 = = 10.94$ Hz against 7.66 Hz), which indicates that the equivalent structural model is somewhat too stiff in bending. The reduced separation between the bending and torsion frequencies in the present model is consistent with the lower predicted flutter speed, since closer modal frequencies promote an earlier bending–torsion coalescence. The higher flutter frequency (14.72 Hz against 11.1 Hz) follows from the same elevated structural frequencies. Overall, the predicted flutter velocity and frequency remain within the same physical order of magnitude as the benchmark solutions.

The discrepancies relative to the reference data can be traced to three classes of simplifying assumptions. The first is structural: the model retains only one bending and one torsional degree of freedom, so that all higher structural modes are neglected, and the equivalent finite-element model does not reproduce exactly the distributed stiffness and inertia of the canonical Goland wing. The second is aerodynamic: the formulation employs the classical two-dimensional Theodorsen theory under incompressible thin-airfoil assumptions, without any distributed spanwise aerodynamic modelling and without an aerodynamic influence-coefficient matrix, which is precisely the source of the systematic difference observed between two- and three-dimensional methods in Table 2. The third is modal convergence: reference Goland studies typically employ six to eight structural modes within a multimodal flutter analysis [1], whereas the present model is, by construction, limited to two generalized coordinates.

Despite these limitations, the implemented methodology provides a coherent aeroelastic workflow. It links finite-element structural extraction, generalized compliance and stiffness construction, projected mass modelling, static-divergence prediction, and reduced-frequency-dependent flutter solution. The model captures the dominant bending–torsion coupling mechanism, identifies a flutter-critical configuration, and produces aeroelastic quantities within the correct physical order of magnitude. Therefore, the present formulation is appropriate as a preliminary stability-assessment tool and as a methodological basis for subsequent higher-fidelity developments.

7. CONCLUSIONS AND FUTURE WORK

A reduced-order FEM-based aeroelastic framework has been developed for the prediction of static divergence and flutter and has been demonstrated on the canonical Goland wing. The methodology combines three main components: structural quantities extracted from a finite-element model, reduction to two physically meaningful generalized coordinates, and classical aeroelastic theory using Theodorsen's unsteady thin-airfoil formulation for the aerodynamic loading. The elastic-axis location, generalized compliance matrix, generalized stiffness matrix, and projected mass matrix were obtained from a reduced set of static finite-element analyses performed under unit loads. These quantities were subsequently used to formulate the divergence problem and the flutter eigenvalue problem.

The implemented workflow produced physically interpretable aeroelastic results. For the analyzed configuration, the flutter speed was found to be lower than the divergence speed, indicating that the system is flutter-critical. This result is consistent with the behavior generally reported for the Goland-wing benchmark. However, the present flutter velocity is lower than the published two-dimensional reference values, and the flutter frequency is higher than the corresponding benchmark values. The divergence speed is also higher than the available reference value. These differences

show that the present model should be interpreted as a preliminary reduced-order formulation rather than as a quantitatively converged benchmark solution.

The main source of structural discrepancy is the limited two-degree-of-freedom representation. The torsional frequency is captured with reasonable accuracy, but the first bending frequency is significantly overestimated, indicating that the equivalent model is too stiff in bending. Since flutter is highly sensitive to the relative position of the bending and torsional modes, this discrepancy affects the predicted flutter boundary. A more accurate structural representation requires the inclusion of additional modes and a closer matching of the distributed stiffness and inertia of the canonical Goland wing.

The aerodynamic formulation also imposes important limitations. Theodorsen theory provides a compact and analytically well-established representation of unsteady thin-airfoil aerodynamics, but it is intrinsically two-dimensional and incompressible. Consequently, it does not represent the finite-span effects, tip effects, spanwise aerodynamic coupling, or compressibility effects that influence the Goland-wing benchmark. Although finite-wing corrections to the effective lift-curve slope may improve the predicted flutter speed, a rigorous extension would require a spanwise-distributed aerodynamic formulation or a generalized aerodynamic force matrix dependent on reduced frequency and Mach number.

The present study therefore validates the computational workflow rather than the complete quantitative fidelity of the reduced model. The procedure demonstrates how FEM-derived structural quantities can be coupled with an unsteady aerodynamic model in order to predict divergence and flutter within a compact reduced-order framework. This is an important intermediate step toward the development of a practical aeroelastic stability tool for more complex experimental configurations.

Future work should focus first on structural enrichment. Additional bending and torsional modes should be introduced, preferably by projecting the dynamics onto FEM eigenmodes rather than onto geometrically defined generalized coordinates. A modal-convergence study should be performed to determine the number of modes required for stable flutter predictions. Particular attention should be given to the first bending mode, whose frequency is presently overestimated.

On the aerodynamic side, the current two-dimensional formulation should be extended toward a spanwise-distributed model. A first improvement may be obtained through strip-theory integration with finite-wing and compressibility corrections. A higher-fidelity formulation should employ generalized aerodynamic force matrices obtained from methods such as the Doublet Lattice Method, the Unsteady Vortex Lattice Method, or unsteady CFD. These methods would allow the real and imaginary components of the aerodynamic response to be introduced consistently in the reduced-frequency flutter problem

Received on June 17, 2026

REFERENCES

1. PALACIOS, R., EPUREANU, B. I., *An intrinsic description of the nonlinear aeroelasticity of very flexible wings*, 52nd AIAA Journal, 2011.
2. BISPLINGHOFF, R. L., ASHLEY, H., HALFMAN, R. L., Aeroelasticity, Dover Publications, New York, 1996.
3. THEODORSEN, T., *General theory of aerodynamic instability and the mechanism of flutter*, NACA Report No. 496, 1935.
4. GOLAND, M., *The flutter of a uniform cantilever wing*, *Journal of Applied Mechanics*, **12**, *4*, pp. A197–A208, 1945.
5. FUNG, Y. C., *An introduction to the theory of aeroelasticity*, Dover Publications, New York, 2008.
6. HODGES, D. H., PIERCE, G. A., *Introduction to structural dynamics and aeroelasticity*, 2nd ed., Cambridge University Press, New York, 2011.
7. PATIL, M. J., HODGES, D. H., CESNIK, C. E. S., *Nonlinear aeroelastic analysis of complete aircraft in subsonic flow*, Journal of Aircraft, **37**, *5*, pp. 753–760, 2000.
8. PATIL, M. J., HODGES, D. H., *Flight dynamics of highly flexible flying wings*, Journal of Aircraft, **43**, *6*, pp. 1790–1798, 2006.
9. SHEARER, C. M., CESNIK, C. E. S., *Nonlinear flight dynamics of very flexible aircraft*, Journal of Aircraft, **44**, *5*, pp. 1528–1545, 2007.
10. SOTOUDEH, Z., HODGES, D. H., CHANG, C.-S., *Validation studies for aeroelastic trim and stability analysis of highly flexible aircraft*, Journal of Aircraft, **47**, *4*, pp. 1240–1247, 2010.
11. WANG, Z., CHEN, P. C., LIU, D. D., MOOK, D. T., PATIL, M. J., *Time domain nonlinear aeroelastic analysis for HALE wings*, 47th AIAA/ASME/ASCE/AHS/ASC Structures, Structural Dynamics, and Materials Conference, AIAA Paper 2006-1640, Newport, Rhode Island, USA, May 2006.
12. MURUA, J., PALACIOS, R., GRAHAM, J. M. R., *Applications of the unsteady vortex-lattice method in aircraft aeroelasticity and flight dynamics*, Progress in Aerospace Sciences, **55**, pp. 46–72, 2012.